JOURNAL OF PHYSICAL ORGANIC CHEMISTRY
J. Phys. Org. Chem. 2007; **20:** 716–731
Published online 2 August 2007 in Wiley InterScience
(www.interscience.wiley.com) DOI: 10.1002/poc.1225

Synthesis and structural study of 2′- and 2′,6′-positioned methyl- and nitro-substituted 3-(arylhydrazono)pentane-2,4-diones

Jan Marten,[1] Wilhelm Seichter,[1] Edwin Weber[1]* and Uwe Böhme[2]

[1]Institut für Organische Chemie, TU Bergakademie Freiberg, Leipziger Straße 29, D-09596 Freiberg/Sachsen, Germany
[2]Institut für Anorganische Chemie, TU Bergakademie Freiberg, Leipziger Straße 29, D-09596 Freiberg/Sachsen, Germany

Received 5 February 2007; revised 2 April 2007; accepted 3 May 2007

ABSTRACT: A systematic series of *ortho*-methyl- and nitro-substituted arylhydrazones **2–6** formed by Japp–Klingemann reaction between pentane-2,4-dione and the respective aryldiazonium salts have been synthesized and studied by X-ray crystal structure analysis, with added quantum chemical calculations. The optimized molecular geometries based on DFT calculations, enabling determination of relevant rotational barriers, and the calculated bond and ring critical points, using the method of 'atoms in molecules', were found to correspond with the experimental data, involving specific molecular conformations and hydrogen-bonded ring structure dependent on the *ortho*-substitution, thus making possible reliable structural prediction of this compound class. Copyright © 2007 John Wiley & Sons, Ltd.
Supplementary electronic material for this paper is available in Wiley InterScience at http://www.mrw.interscience.wiley.com/suppmat/0894-3230/suppmat/

KEYWORDS: 3-(arylhydrazono)pentane-2,4-diones; synthesis; crystal structures; DFT calculations

INTRODUCTION

Coupling of a 1,3-dicarbonyl compound with an aromatic diazonium salt to yield an arylhydrazone is a synthetic process commonly known as the Japp–Klingemann reaction.[1] Using this method has given rise to a variety of arylhydrazones that derive from different arylamines and 1,3-dicarbonyl compounds,[1–3] being described as effective complexants for transition metal ions,[3–6] or antineoplastic components.[7] All of them show a characteristic intramolecular hydrogen bridge linking one of the carbonyl groups to the NH-moiety of the hydrazone unit. This has recently been corroborated by X-ray crystal studies.[3,8] It has also been observed that in hydrazones of this type based on an unsymmetrically substituted 1,3-dione, the six-membered H-bonded ring will always be generated at the steric most favorable side of the molecule.[9] Moreover, as shown from the crystal structures,[3,8] the carbonyl groups are in a conformational *anti* position. On the other hand, tautomerism, which is a typical feature of 1,3-dicarbonyl compounds,[10] has not yet been proved to exist in respective arylhydrazones, although implying a promising target for the design of functional materials attributed to smart hydrogen bonding[11] or photo-triggered structural switching.[12]

Substitution in the *ortho* positions of the aryl ring relative to the hydrazone function of **1** might be another parameter of influence to control structural properties of this compound class. Thus the series of arylhydrazones **2–6** (Scheme 1) featuring dimensionally similar but electronically different methyl and nitro groups in a systematic pattern of substitution have been synthesized and structurally studied, including DFT calculations of the geometric facts.

RESULTS AND DISCUSSION

Synthesis

The hydrazones **1–6** (Scheme 1) were synthesized via Japp–Klingemann reaction[1] between the respective aromatic diazonium salts and pentane-2,4-dione in a methanolic solution containing sodium acetate.[3] The diazonium salts were obtained by usual diazotation of the corresponding aniline.[13]

**Correspondence to:* E. Weber, Institut für Organische Chemie, TU Bergakademie Freiberg, Leipziger Straße 29, D-09596 Freiberg/Sachsen, Germany.
E-mail: edwin.weber@chemie.tu-freiberg.de

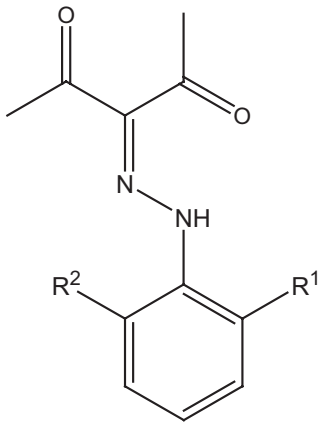

1	$R^1 = H$, $R^2 = H$
2	$R^1 = CH_3$, $R^2 = H$
3	$R^1 = CH_3$, $R^2 = CH_3$
4	$R^1 = NO_2$, $R^2 = H$
5	$R^1 = NO_2$, $R^2 = NO_2$
6	$R^1 = CH_3$, $R^2 = NO_2$

Scheme 1. Compounds discussed

X-ray structural study

Relating to the problem, crystal structures of six 3-(arylhydrazono)pentane-2,4-diones containing *ortho*-substituents of different electronic nature have been studied. They involve the unsubstituted parent compound **1**, its 2-methyl and 2,6-dimethyl-substituted analogs **2** and **3**, the 2-nitro and 2,6-dinitro derivatives **4** and **5** as well as the 2-nitro-6-methylarylhydrazone **6**. Relevant crystallographic data are summarized in Table 1. A selection of bond distances and angles including hydrogen bond parameters is given in Tables 2 and 3, respectively. ORTEP plots of the molecules **1**, **5**, and **6** are displayed in Fig. 1. The packing diagrams of compounds **1** and **6** are illustrated in Figs 2 and 3, respectively. Packing diagrams of **2–5** are given in Figs SI–SIV, respectively.

A common feature of the compounds is the presence of an intramolecular six-membered π-conjugated hydrogen-bonded ring containing an extraordinary strong N—H···O hydrogen bond with N···O bond distances ranging over 2.542(3) and 2.597(2) Å. Investigations based on the Resonance Assisted Hydrogen Bond (RAHB) model, which were applied to related compounds by Gilli *et al.*,[14] suggests a synergistic mutual reinforcement of intramolecular hydrogen bonding and π-delocalization within structure elements like the H—N—N=C—C=O system. This model, however, is criticized recently.[15] On the other hand, calculations have shown that the π-electron delocalization in a related system correlates well with parameters describing the H-bond strength such as the electron density at the H···O bond critical point.[16] Characterization of the present crystal structures therefore should be focused on how electronic properties of the aryl substituents influence bonding parameters and thus π-electron delocalization within the conjugated system and to what extent the molecular conformation is affected by non-covalent intermolecular interactions, hence supplying potential reasoning for clearing up this point in dispute.

Molecular structures. All molecules adopt the *EZE*-conformation which represents, in this order, the alignment of the non-H-bridged O(2)=C(4), the hydrogen-bonded O(1)=C(2) fragment, and the aryl group with respect to the C(3)=N(1) double bond.[17] Previous studies revealed that this conformation is also preferred in the solid phase structures of other compounds of this kind.[8,2,18] The H-bridged hydrazone ring and the aromatic ring in the compounds deviate more or less from coplanarity. The dihedral angles between the least-squares planes of these molecular units (Scheme 2) range between 2.5(1) and 17.2(2)°, being largest for the 2,6-dinitroarylhydrazone, **5** for reasons which will be discussed below.

Table 2 reflects the general relationship between bond lengths within the C(3)-N(1)-N(2)-C(6) sequence of the compounds showing that a relative increase of the N(1)—N(2) bond length corresponds with a decrease of the respective N(2)—C(6) and N(1)—C(3) bond lengths. Furthermore, the trend of the N(2)···O(1) distances indicates that electron-donating *ortho*-substituents of the aromatic ring tend to strengthen the intramolecular hydrogen bond whereas it is weakened by electron-withdrawing groups. Another interesting feature concerns the bond angle at C(3) which includes a significant decrease of the angle N(1)–C(3)–C(4) [112.2(3)–114.0(1)°] accompanied by an increase of the angle N(1)–C(3)–C(2) [122.5(2)–124.9(1)°]. It is evident from Tables 2 and 3 that these variations depend on the electronic character of the substituents and correlate with hydrogen bond parameters.

Compound **1** (Fig. 1a) exhibits a nearly planar overall conformation with bond distances and angles which are similar to those found in other non-functionalized β-diketoarylhydrazones.[18] Surprisingly, introduction of methyl groups in the *ortho* position of the aromatic ring, as in **2** and **3,** have only little influences on the molecular conformation and bond parameters. Also, the presence of the electron-withdrawing nitro group in **4** hardly affects the distance N(2)···O(1), being very similar to that of **1,** although in **4** the hydrogen at N(2) is involved in a bifurcated intramolecular hydrogen bond with the nitro group [(N(2)···O(3), 2.617(7) Å], forcing the substituent into coplanarity with the aromatic ring. Interestingly, in the monosubstituted compounds **2** and **4** with potential *syn* or *anti* position of the substituent (CH_3, NO_2) relative to the nitrogen atom N(1), only the *anti* conformation is shown. This is reasonable for compound **4** due to the nitro group participating in a bifurcated hydrogen bond, unlike the methyl substituent in compound **2** being unable in this

DOI: 10.1002/poc

Table 1. Crystallographic and structure refinement data of the compounds studied

Compound	**1**	**2**	**3**	**4**	**5**	**6**
Empirical formula	$C_{11}H_{12}N_2O_2$	$C_{12}H_{14}N_2O_2$	$C_{13}H_{16}N_2O_2$	$C_{11}H_{11}N_3O_4$	$C_{11}H_{10}N_4O_6$	$C_{12}H_{13}N_3O_4$
Formula weight	$M_r = 204.23$	$M_r = 218.25$	$M_r = 232.28$	$M_r = 249.23$	$M_r = 294.23$	$M_r = 263.25$
Crystal system	Triclinic	Triclinic	Monoclinic	Triclinic	Monoclinic	Monoclinic
Space group	*P*-1	*P*-1	*C*2/*c*	*P*-1	*Cc*	*P*2(1)/n
a (Å)	4.2210(1)	8.1494(3)	14.694(3)	7.21820(10)	8.2901(5)	11.154(2)
b (Å)	10.950(2)	8.6157(3)	16.603(3)	8.2163(2)	20.7103(13)	8.200(2)
c (Å)	12.468(3)	9.3452(3)	11.065(2)	11.4241(2)	7.5758(4)	14.065(3)
α (°)	68.513(11)	74.583(2)	90.00	70.0590(10)	90.00	90.00
β (°)	84.452(11)	65.821(2)	112.49(3)	87.6630(10)	105.953(4)	102.11(3)
γ (°)	89.907(11)	83.380(2)	90.00	65.1290(10)	90.00	90.00
V (Å^3)	533.36(19)	577.03(3)	2494.2(8)	573.636(19)	1250.60(13)	1257.8(5)
Z	2	2	8	2	4	4
F(000)	216	232	992	260	608	552
D_c (Mg/m^3)	1.272	1.256	1.237	1.443	1.563	1.390
μ (mm^{-1})	0.089	0.087	0.684	0.112	0.130	0.898
Data collection						
Temperature (K)	298(2)	298(2)	293(2)	296(2)	93(2)	293(2)
No. of collected reflections within the θ-limit (°)	7615	15698	3428	16391	16808	2694
Index ranges $\pm h$, $\pm k$, $\pm l$	−3.4; ±12; ±14	±11; ±12; ±13	−4,18; 0,20; ±13	±11; ±12; ±17	±11; ±29; ±10	0,13; −10,0; ±17
No. of unique reflections	1669	3370	2535	4322	3740	2567
R_{int}	0.0537	0.0225	0.0702	0.0163	0.0346	0.0184
Refinement calculations	Full-matrix least-squares on all F^2 values					
Weighting expression w[a]	$1/[s^2(F_o^2)+(0.1000P)^2+0.4105P]$	$1/[s^2(F_o^2)+(0.0000P)^2+0.0000P]$	$1/[s^2(F_o^2)+(0.1476P)^2+1.0343P]$	$1/[s^2(F_o^2)+(0.0869P)^2+0.0000P]$	$1/[s^2(F_o^2)+(0.1000P)^2+0.8356P]$	$1/[s^2(F_o^2)+(0.1188P)^2+0.4305P]$
No. of refined parameters	142	152	154	166	196	172
No. of *F* values used [$I > 2\sigma(I)$]	813	2421	1636	3480	3160	1783
Final *R*-indices						
$R(=\Sigma\|\Delta F\|/\Sigma\|F_o\|)$	0.0467	0.0485	0.0883	0.0458	0.0368	0.0706
wR on F^2	0.1869	0.0891	0.2195	0.1642	0.1099	0.2261
S (=Goodness of fit on F^2)	0.800	1.255	1.045	1.442	0.909	1.106
Final $\Delta\rho_{max}/\Delta\rho_{min}$ (e/Å^3)	0.15/−0.15	0.20/−0.17	0.45/−0.33	0.33/−0.22	0.25/−0.18	0.35/−0.38

[a] $P = (F_o^2 + 2F_c^2)/3$.

DOI: 10.1002/poc

Table 2. Selected conformational parameters of the compounds **1–6**

Compound	1	2	3	4	5	6
Bond lengths (Å)						
N(1)—N(2)	1.301(4)	1.297(1)	1.284(3)	1.314(1)	1.333(2)	1.312(3)
N(1)—C(3)	1.321(4)	1.321(1)	1.333(3)	1.314(1)	1.307(2)	1.317(4)
N(2)—C(6)	1.414(4)	1.411(1)	1.418(3)	1.397(1)	1.386(2)	1.389(3)
C(2)—C(3)	1.469(5)	1.470(1)	1.488(4)	1.484(1)	1.495(2)	1.478(4)
C(3)—C(4)	1.476(5)	1.473(1)	1.465(4)	1.487(1)	1.498(2)	1.485(4)
C(2)—O(1)	1.234(4)	1.230(1)	1.234(3)	1.229(1)	1.226(2)	1.226(4)
C(4)—O(2)	1.219(4)	1.207(1)	1.215(3)	1.211(1)	1.216(2)	1.212(4)
Bond angles (°)						
C(3)—N(1)—N(2)	122.4(3)	121.31(9)	121.5(2)	121.52(6)	120.01(14)	120.1(2)
N(1)—N(2)—C(6)	119.4(3)	120.77(9)	124.7(2)	118.02(6)	118.82(13)	122.5(2)
N(1)—C(3)—C(2)	123.7(3)	123.41(10)	122.5(2)	124.21(7	124.86(14)	123.5(3)
N(1)—C(3)—C(4)	112.2(3)	112.92(9)	113.9(2)	112.30(7)	113.96(14)	113.9(3)
C(2)—C(3)—C(4)	124.1(3)	123.65(9)	123.6(2)	123.50(7)	121.16(14)	122.6(3)
C(3)—C(2)—O(1)	119.1(3)	119.80(10)	119.3(2)	118.91(7)	119.17(15)	119.7(3)
C(3)—C(4)—O(2)	121.2(3)	122.65(10)	121.7(3)	121.66(10)	119.68(15)	121.7(3)
Torsion angles (°)						
O(1)–C(2)–C(3)–N(1)	−5.5(5)	−5.21(17)	−0.9(4)	0.22(13)	14.1(3)	−7.5(5)
C(2)–C(3)–N(1)–N(2)	3.6(5)	1.87(16)	−0.1(4)	−0.99(12)	−6.0(3)	1.8(4)
C(3)–N(1)–N(2)–C(6)	−178.8(3)	−177.37(9)	−179.7(2)	179.63(6)	177.30(15)	−178.4(2)
C(2)–C(3)–C(4)–O(2)	−9.5(5)	−6.30(18)	1.8(5)	5.06(15)	26.6(3)	−12.8(5)
Dihedral angle (°)						
mpla(1)[a]···mpla(2)[b]	3.53(0.88)	5.1(0.27)	3.35(0.57)	2.47(0.10)	17.72(0.18)	7.13(0.18)
mpla(1)[a]···mpla(3)[c]	—	—	—	3.02(0.14)	67.04(0.08)	74.42(0.19)
mpla(1)[a]···mpla(4)[d]	—	—	—	—	8.70(0.09)	—

[a] The mpla(1) means the mean plane given by C(6)-C(7)-C(8)-C(9)-C(10)-C(11).
[b] mpla(2) means the mean plane given by the sequence H(2)-N(2)-N(1)-C(3)-C(2)-O(1).
[c] mpla(3) means the mean plane given by N(3)-O(3)-O(4) in **4**, **5**, **6**.
[d] mpla(4) means the mean plane given by N(4)-O(5)-O(6) in **5**.

respect. Possibly, also a steric interference between the *ortho*-substituent and the N(1) atom in the *syn* position is a barrier to form this conformer. Additional indication to this fact is that in compounds **3**, **5**, and **6** having an *ortho*-disubstituted aromatic ring, substituent-induced intramolecular strain causes a marked decrease of the bond angle N(2)–C(6)–C(11) whereas the N(2)–C(6)–C(7) angle is increased. This effect is most distinctive in the dimethyl derivative **3**, in which these angles are 113.3 and 124.4°, respectively. In the 2,6-disubstituted compounds **5** and **6**, the nitro group at C(7) is inclined with regard to the aromatic plane resulting in reduction of intramolecular strain to give more regular bonding angles at C(6).

In the crystal structure of **5** (Fig. 1b), the molecule exhibits a highly bent geometry along the C_5O_2 fragment which can be seen from enlarged torsion angles of the atomic sequences N(1)-C(3)-C(2)-O(1) and C(2)-C(3)-C(4)-O(2) being 14.1(3) and 26.6(3)°, respectively. The H-bridged hydrazone ring, however, is less affected by this distortion. The largest atomic distance from its mean plane is found for atoms N(2) and C(3) being only 0.07(1) and 0.06(1) Å apart. Similar to the monosubstituted compound **4**, one of the nitro groups in **5** is involved in an intramolecular bifurcated hydrogen bond [(N(2)···O(1), 2.597(2) Å] and thus is nearly coplanar with the aromatic ring [$\Theta = 8.7(1)°$], while the other nitro group, not being involved in hydrogen bonding, is rotated 67.0(1)° out of the aromatic plane.

Unlike **4** and **5**, the nitro substituent of compound **6** (Fig. 1c) is arranged *syn* with respect to N(1) and therefore excluded from intramolecular hydrogen bond interaction. Hence **6** corresponds in the parameters of hydrogen bonding with compound **3**. Moreover, a distinct twist [74.4(2)°] of the nitro group of **6** out of the aromatic ring plane prevents from mutual interaction of the aromatic and nitro π-electrons.

Packing structures. Due to the planar geometry, the crystal structures of all studied compounds, excepting compound **6**, are characterized by a sheet-like alignment of molecules of which Fig. 2 is illustrating a representative example. As the molecules lack strong outwardly H donor sites, intermolecular cross-linking is restricted to C—H···O contacts and $\pi\cdots\pi$ stacking interactions which, however, give rise to specific types of supramolecular pattern.

In the crystal structure of **1** (Fig. 2), the molecules are linked together to double strands running along the crystallographic *b*-axis. Both carbonyl oxygens are involved in hydrogen bonding to the aromatic parts of neighboring molecules [O(1)···H(11), 2.55 Å; O(2)···H(9), 2.63 Å]. Offset arene–arene π-contacts with a separation of 4.22 Å

DOI: 10.1002/poc

Table 3. Distances (Å) and angles (deg.) of hydrogen bond interactions of **1–6**

Atoms involved		Distances			Angle
D–H···A	Symmetry	D···H	D···A	H···A	D–H···A
(1)					
N(2)–H(2)···O(1)	x, y, z	0.91	2.580(4)	1.85	136.4
C(9)–H(9)···O(2)	$-1+x, -1+y, z$	0.96	3.582(5)	2.63	171.5
C(11)–H(11)···O(1)	$-x, 1-y, -z$	0.93	3.461(5)	2.55	167.3
(2)					
N(2)–H(2)···O(1)	x, y, z	0.94	2.562(1)	1.82	134.3
C(9)–H(9)···O(2)	$1+x, 1+y, -1+z$	0.93	3.499(2)	2.58	168.1
(3)					
N(2)–H(2)···O(1)	x, y, z	0.86	2.538(9)	1.85	136.8
C(10)–H(10)···O(2)	$0.5+x, 0.5-y, -0.5+z$	0.93	3.384(5)	2.48	163.9
(4)					
N(2)–H(2)···O(1)	x, y, z	0.79	2.578(1)	2.02	127.6
N(2)–H(2)···O(3)	x, y, z	0.79	2.617(1)	2.01	132.7
C(10)–H(10)···O(2)	$x, y, -1+z$	0.93	3.269(1)	2.64	125.3
C(8)–H(8)···O(3)	$x, -1+y, z$	0.93	3.344(1)	2.56	141.8
(5)					
N(2)–H(2)···O(1)	x, y, z	0.79	2.597(2)	2.01	130.9
N(2)–H(2)···O(5)	x, y, z	0.79	2.605(2)	2.01	130.4
C(1)–H(1B)···O(2)	$x, 1-y, 0.5+z$	0.98	3.411(2)	2.57	143.2
C(1)–H(1A)···O(4)	$1+x, y, z$	0.98	3.123(2)	2.64	139.3
C(5)–H(5A)···O(3)	$x, 1-y, -0.5+z$	0.98	3.578(2)	2.63	163.1
C(1)–H(1A)···O(6)	$0.5+x, 0.5-y, 0.5+z$	0.98	3.323(2)	2.53	138.2
C(5)–H(5C)···O(6)	$-0.5+x, 0.5-y, -0.5+z$	0.98	3.423(2)	2.46	167.6
(6)					
N(2)–H(2)···O(1)	x, y, z	0.86	2.542(3)	1.86	135.3
C(1)–H(1A)···O(3)	$0.5+x, 0.5-y, 0.5+z$	0.96	3.442(5)	2.64	140.9

(centroid-to-centroid) stabilize the crystal packing in direction of the *a*-axis.

A similar layered arrangement of molecules is also found in the crystal structures of the methyl derivatives **2** (Fig. SI) and **3** (Fig. SII). The presence of methyl groups, however, restricts intermolecular hydrogen bonding to the oxygen O(2) forming either linear (**2**) or zigzag (**3**) C—H···O bonded single strands. In the structure of **2**, the aromatic rings and the H-bonded six-membered rings are arranged in a stacking mode, which suggests attractive forces between them. Obviously, non-aromatic molecular entities featuring a conjugated π-electron system can replace aromatic rings in this specific $\pi\cdots\pi$ stacking arrangement. By way of contrast, in the crystal structure of **3**, only the H-bonded six-membered rings are subjected to stacking interactions, possibly because of the sterical barrier of the *ortho*-substituents, which prevents effective face-to-face aromatic interactions.

In the compounds **4–6**, the nitro substituents provide additional coordination sites which allow a higher degree of intermolecular cross-linking. In the crystal structure of the monosubstituted derivative **4** (Fig. SIII), only one of the nitro oxygens takes part in an intramolecular N—H···O and a weaker C—H···O contact to an adjacent

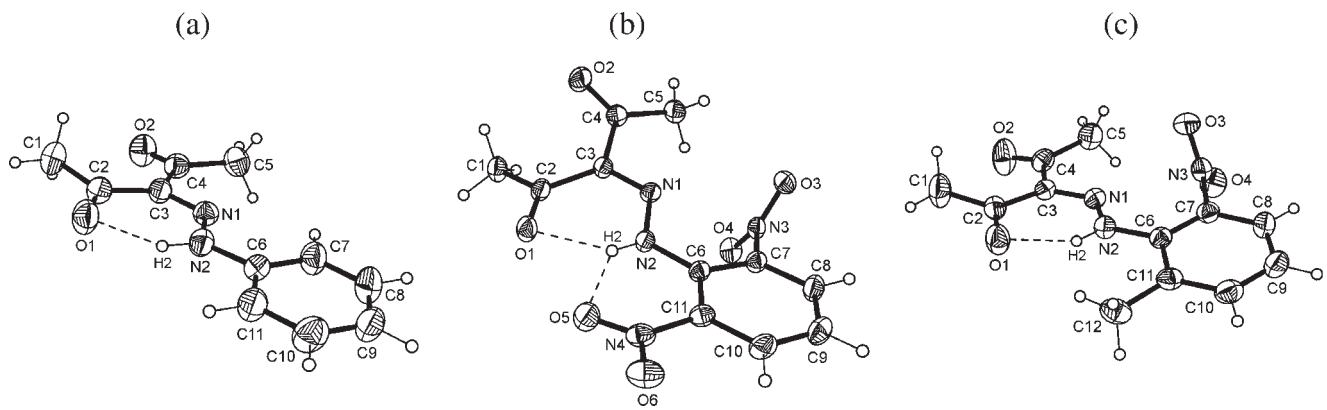

Figure 1. ORTEP plots of the molecular structures of compounds **1** (a), **5** (b), and **6** (c). The thermal ellipsoids are drawn at the 50% probability level and the hydrogen bonds are shown as broken lines

DOI: 10.1002/poc

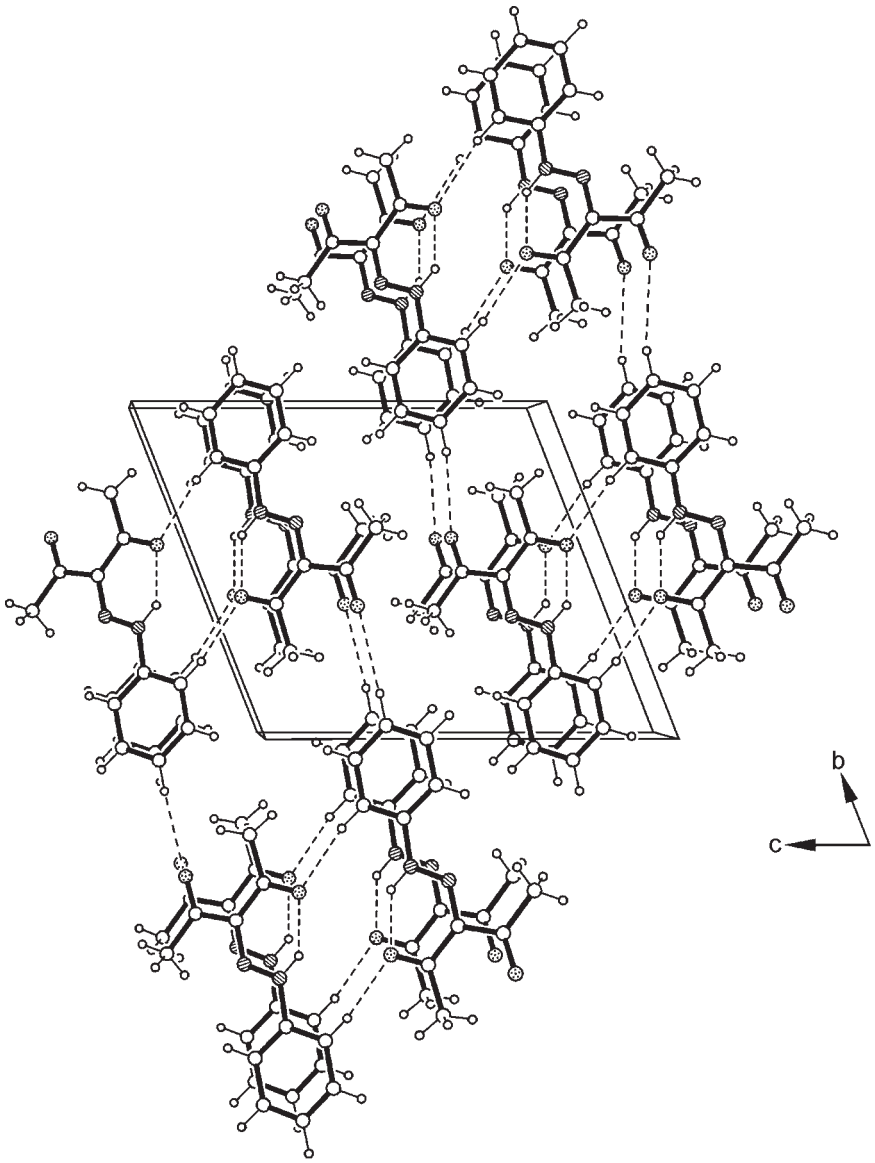

Figure 2. Packing diagram of **1** viewed down the crystallographic *a*-axis. The hydrogen bonds are shown as broken lines

molecule. Attachment of an additional nitro substituent, as in the 2,6-dinitro-substituted compound **5** (Fig. SIV) drastically changes the molecular assembly in the crystal. With the exception of the nitro oxygen O(5), which is involved in intramolecular hydrogen bonding, all other strong acceptors are involved in intermolecular cross-linking, thus stabilizing the crystal structure by a close network of non-covalent interactions. Different from the crystal structures described above, the 2-nitro-6-methyl-substituted derivative **6** shows a typically columnar packing mode with the molecules of the neighboring stack inclined to one another (Fig. 3).

DFT calculations

Quantum chemical calculations have been performed to obtain a better insight into the structural features of the compounds under investigation. Optimized geometries are denoted with formula number and following letters (**a** or **b**) in order to distinguish calculated geometries from experimental data.

Parent compound 1 and methyl-substituted derivatives 2 and 3. A comparison of the optimized geometry of **2a** with the X-ray structure of **2** shows very good agreement of bonding parameters (Fig. 4a). There are only small deviations in the overall geometry of the molecule with respect to the angle between the planes 1 and 2 (Scheme 2) formed by the hydrazone unit (plane 1) and the phenyl ring including *ortho*-substituents (plane 2). The optimized molecule **2a** is completely planar while the molecule **2** in the solid state shows an angle of 3.53°(0.88) between both planes. This difference is more pronounced in the structure overlay of **3a** and **3**. The angle between the planes of **3** in the solid state is 3.35°(0.57).

DOI: 10.1002/poc

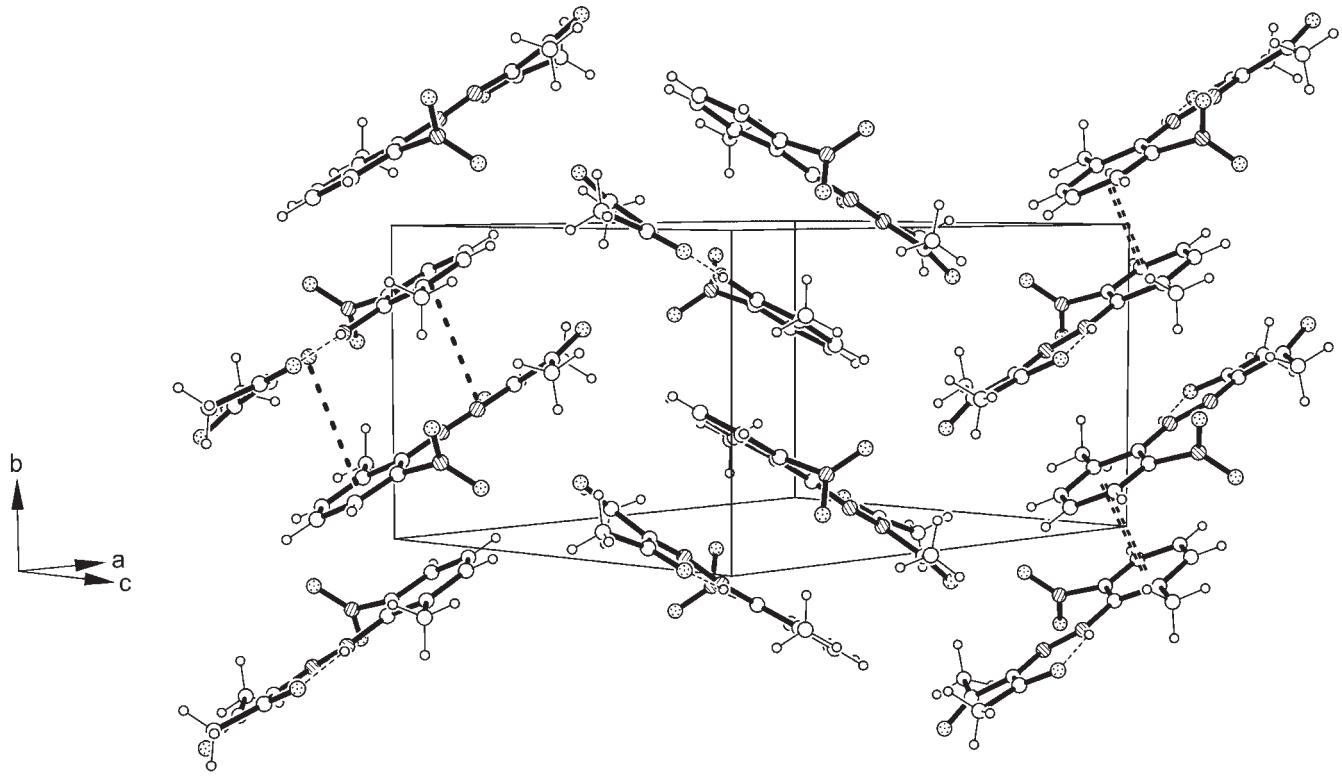

Figure 3. Packing diagram of **6**. Hydrogen bonds are shown as broken single lines; arene–arene interactions are marked as broken double lines; interactions between aromatic rings and H-bridged hydrazone rings are displayed as dotted lines

On the other hand, the optimized geometry of the molecule in the gas phase (**3a**) has an angle of 21.14° between planes 1 and 2. This non-planar geometry of the unhindered molecule in the gas phase suggests a repulsive steric interaction between the methyl groups in *ortho* positions of the phenyl ring and the hydrazone unit.

The quantum chemical investigation of rotational barriers is a suitable tool to investigate such kind of steric interactions more closely.[19] For that purpose, relaxed potential energy surface (PES) scans have been performed with rotation of the phenyl group around the bond N(2)—C(6), being schematically shown for **1a**, **2a**, and **3a** in Fig. 5. We can assume that all steric and electronic interactions between the phenyl groups and the hydrazone unit are switched off at a torsion angle of 90°. Therefore the torsional potentials of **2a** and **3a** were scaled in that way that all three functions intersect at 90°. It is possible to draw information about the different steric interactions of **1a**, **2a**, and **3a** by comparing these graphs.

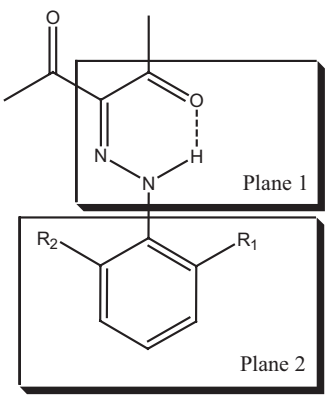

Scheme 2. Representation of planes discussed in the text

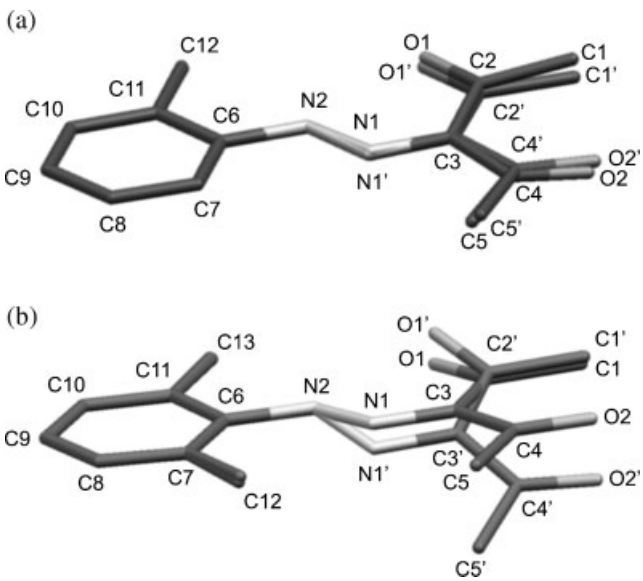

Figure 4. Structure overlay of the optimized geometries of **2a** (a) and **3a** (b) with the geometries of **2** and **3** from X-ray structures, respectively. The aromatic carbon atoms of the arene unit were positioned on top of each other

DOI: 10.1002/poc

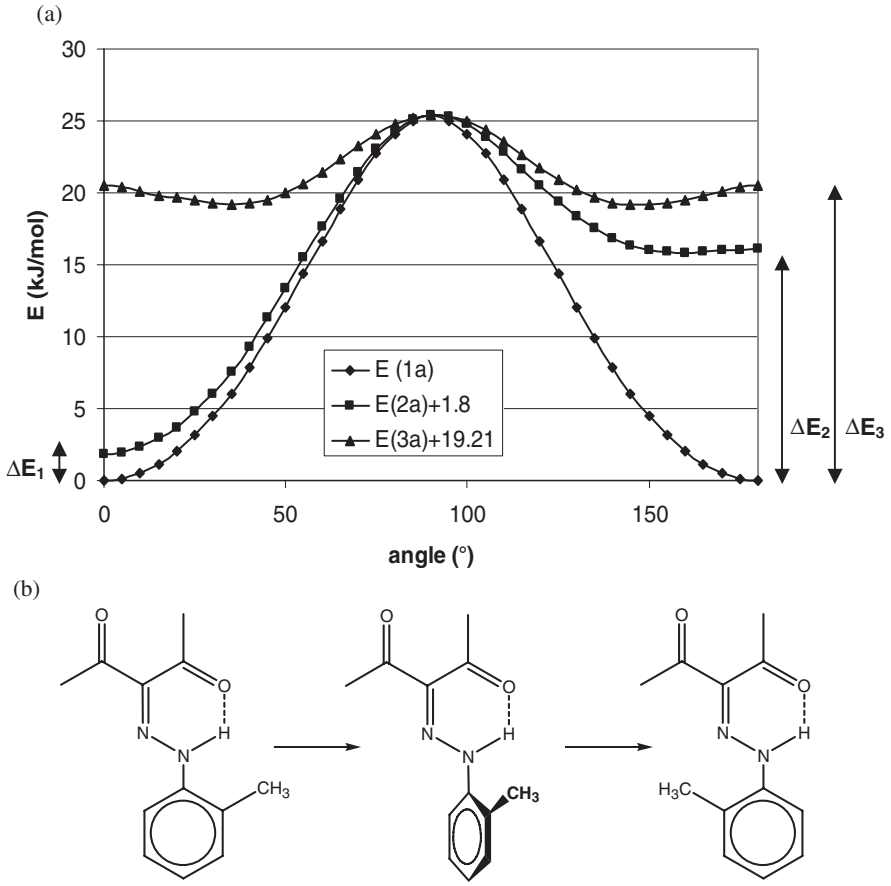

Figure 5. Schematic representation (a) of PES scans of **1a**, **2a**, and **3a** for rotation of the aryl ring around N(2)–C(6). Illustration (b) of the rotational conformers of **2a**

The torsional potential for **1a** gives information about the conjugative interaction between the π-system of the phenyl ring and the hydrazone unit. This torsional potential has a maximum at 90°, with 25.4 kJ/mol higher energy than the molecule in its minimum geometry with a torsion angle of 0°. The substitution of one *ortho* position at the phenyl ring of **1** by a methyl group, as in **2**, leads to torsion potential with two different minima [E(**2a**) in Fig. 5]. The global minimum of this molecule is at a torsion angle C(7)–C(6)–N(2)–N(1) of 0°. This global minimum is 1.8 kJ/mol higher in energy than the global minimum for **1a** ($\triangle E_1$ in Fig. 5) thus indicating that there is only a small steric repulsion. The maximum is also at 90° due to the complete inhibition of conjugative interaction. Going further to 180° leads to a local minimum which is 14.3 kJ/mol higher in energy than the global minimum. This can be explained with the repulsive interaction between the methyl group in *ortho* position and the free electron pair at N(1). The steric repulsion between the methyl group and the nitrogen atom N(1) can be estimated with 16.1 kJ/mol ($\triangle E_2$ in Fig. 5). The rotational barrier is changed, if there are two methyl groups in both *ortho* positions of the phenyl ring. The global minimum is no longer at a torsion angle of 0°, but at a torsion angle of about 35°. This conformation is obviously the best compromise between minimal steric repulsion and optimal conjugative interaction. The overall rotational barrier of **3a** is much smaller than for the molecules discussed before. This can be attributed to the steric repulsion between the methyl groups in both *ortho* positions with the hydrazone unit which disfavors torsion angles close to 0 or 180°. The steric repulsion between two methyl groups in *ortho* position and the hydrazone unit can be estimated with 21 kJ/mol ($\triangle E_3$ in Fig. 5). The respective torsion angle for **3** is much smaller in the solid state [3.4(0.6)° between the mean plane given by C(6)-C(7)-C(8)-C(9)-C(10)-C(11) and the mean plane given by the sequence H(2)-N(2)-N(1)-C(3)-C(2)-O(1)], suggesting a consequence of packing effects. However, one should bear in mind that these values were calculated for an isolated molecule in the gas phase and depend also on the method and basis set combination. Therefore, these values should be regarded as a *qualitative description* of the rotational barrier and the electronic and steric effects connected with this rotation.

Nitro-substituted compounds 4 and 5. The structure overlay of the optimized geometry of **4a** with the geometry of **4** from X-ray structure analysis shows a nearly perfect fit (Fig. 6a), which is a remarkable case where gas phase and solid state molecular geometry closely correspond. The molecule is completely planar

DOI: 10.1002/poc

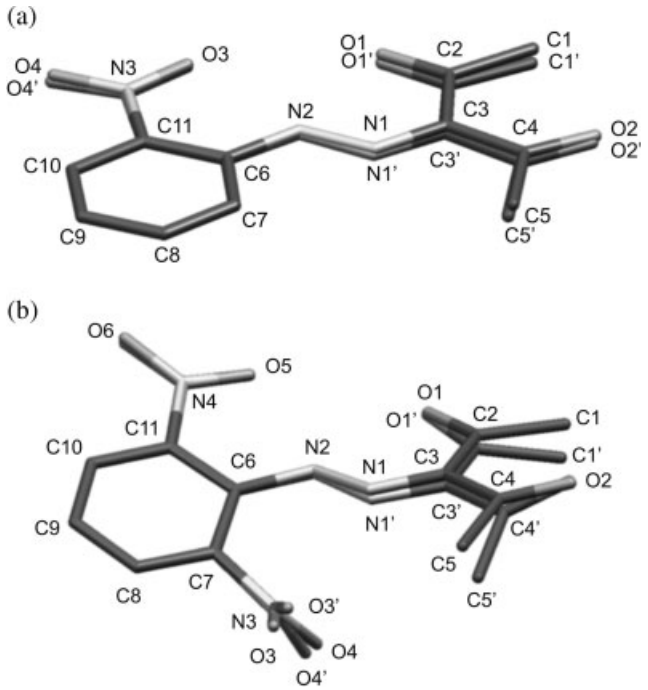

Figure 6. Structure overlay of the optimized geometries of **4a** (a) and **5a** (b) with the geometries of **4** and **5** from X-ray structures, respectively. The aromatic carbon atoms were positioned on top of each other

allowing maximal conjugation of the π-system. Furthermore, a bifurcated hydrogen bond from N(2)—H(2) to O(1) and O(3) is indicated on the basis of the structural data (*cf*. Fig. SIII). To obtain some information about these stabilizing effects, three different torsion potentials have been investigated: (a) the rotation of the phenyl ring around the bond N(2)—C(6); (b) the rotation of the nitro group around the bond C(11)—N(3); (c) the rotation of the carbonyl group at C(2)—O(1) around C(2)—C(3).

The rotational barrier of the phenyl ring around the bond N(2)—C(6) of **4a** gives a PES (Fig. 7) which is similar to the rotation of the phenyl ring in **2a**. There is a global minimum at 0° and a local minimum at 155°. The maximum is at 95°, which is 32.9 kJ/mol higher in energy compared to the global minimum. Rotation of the nitro group out of the planar conformation not only reduces π-conjugation with the phenyl ring but also breaks the hydrogen bond. This barrier amounts to 23.6 kJ/mol for **4a**, a value which is very similar to the barrier of nitrobenzene (24.2 kJ/mol).[20] Hence, from this data there is no remarkable effect which could be ascribed to the presence of a hydrogen bond between N(3)—O(3) and H(2)—N(2). Rotation of the carbonyl group by varying the torsion angle O(1)–C(2)–C(3)–N(1) impairs both the π-conjugation of the 3-(hydrazono)pentane-2,4-dione unit and the potential hydrogen bond between O(1) and N(2)—H. The total energy of the molecule increases about 22.6 kJ/mol when this torsion angle is at 90°. The intramolecular H-bond energy for ketohydrazones was estimated with 29.4 kJ/mol at the B3LYP/6-31 + G(d,p) level in a previous work.[21] Further rotation results in a continuing increase of energy since the methyl group at C(1) comes into spatial conflict with H(2).

The PES scan of **5a** was scaled to have the same maximum energy as the PES scan of **4a** (Fig. 7). The rotation of the phenyl ring around the bond N(2)—C(6) of **5a** gives a symmetric PES with two minima at 30 and 150°. These minima represent the best compromise between (a) steric repulsion between the nitro group and the free electron pair at N(1), (b) the attractive interaction between one oxygen atom of the nitro group and H(2), and (c) the maximized conjugative interaction between phenyl ring and the hydrazono group. The maximum of this PES scan is at 90° with 26.2 kJ/mol higher energy than the minima. All three interactions mentioned above are switched off at 90°. Only the nitro groups attain maximal conjugative interaction with the phenyl ring at this torsion angle.

A comparison of the PES scans of **4a** and **5a** allows to draw some interesting conclusions. The energy difference $\triangle E_4$ represents the destabilizing effect between the nitro group and the free electron pair at N(1) and can be estimated to 6.5 kJ/mol in these compounds. The energy difference $\triangle E_5$ can be interpreted as the stabilizing effect between one oxygen atom of the nitro group and H(2) with a value of 10.1 kJ/mol.

In order to obtain more information about the bonding situation in 3-(arylhydrazono)pentane-2,4-diones, including possible hydrogen bonds, another method of quantum chemical analysis has been used. Compound **4a** which shows a remarkably close fit to the solid state structure was chosen as a representative example. For that purpose, the Atoms in Molecules (AIM) Theory can be utilized.[22] This method partitions the electron density of a molecule into individual non-overlapping atomic fragments by rigorously defined interatomic surfaces.[23] Various properties can be derived from the electron density distribution. The electron density in a molecule is a three-dimensional function which has four types of extrema: maxima, minima, and two types of saddle points.[24] The maxima coincide with the nuclear positions. Minima are found in the center of cage molecules and are called cage critical points. Saddle points being specific to a maximum in one dimension and a minimum in two dimensions are called ring critical points. These are found in the center of atomic rings. Saddle points resulting from a maximum in two dimensions and a minimum in one dimension are called bond critical points. When a bond critical point is found between two atoms, we can draw an atomic interaction line. When the molecule is in an equilibrium geometry, the atomic interaction line is called a bond path. A bond path, however, is not identical with a bond in the sense used by Lewis. Bond paths of this particular type are observed for predominately ionic bonds, covalent bonds, weak hydrogen bonds, and even interactions between anions. Unfortunately, the topological analysis of electron density cannot discriminate between attractive

DOI: 10.1002/poc

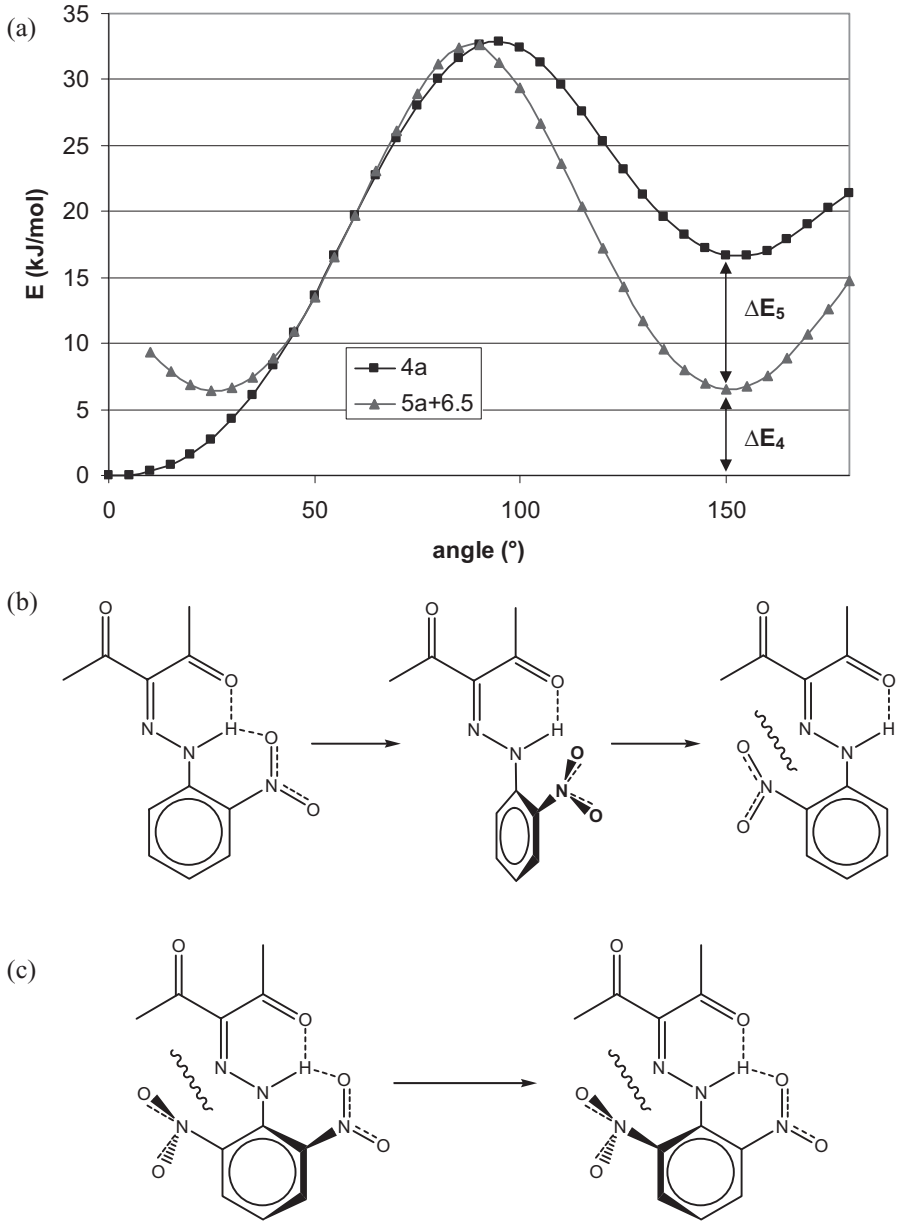

Figure 7. Schematic representation (a) of PES scans of **4a** and **5a** for the rotation of the aryl ring around N(2)–C(6). Illustration of the conformational rotation of **4a** (b) and **5a** (c), with attractive interactions symbolized by a broken line, repulsive interactions by a zigzag line

and repulsive interactions but tells us that *there are interactions* between the atoms, discussed in more detail in recent literature.[25–28] In order to avoid improper conclusions from the topological analysis of electron density, the calculated torsional potentials from above are supportive, allowing us to distinguish unambiguously between attractive and repulsive interactions.

Figure 8a shows the electron density distribution of **4a** in the plane of the atoms. The AIM analysis allows to derive a molecular graph which is shown in Fig. 8b. The atoms are connected by atomic interaction lines going through the bond critical points. These lines correspond widely to our association of covalent bonds in this organic molecule. There are distinct properties of the electron density at the bond critical points that provide us with useful information about the nature of the bond.[24] The first property is the value of the electron density, which is given in atomic units (e/Bohr^3) in Table 4. It is possible to draw conclusions about the bonding degree (single/double/triple bond) by comparing this value with suitable reference molecules. The second value is the ellipticity, which represents the shape of the electron density distribution in a plane perpendicular to the bond path at the bond critical point. While double bonds show significant bond ellipticity, single and triple bonds do not.

The bond critical point between C(2) and O(1) of **4a** has electron density of 0.40 e/Bohr^3 and a very small bond ellipticity between. These values are very similar to the

DOI: 10.1002/poc

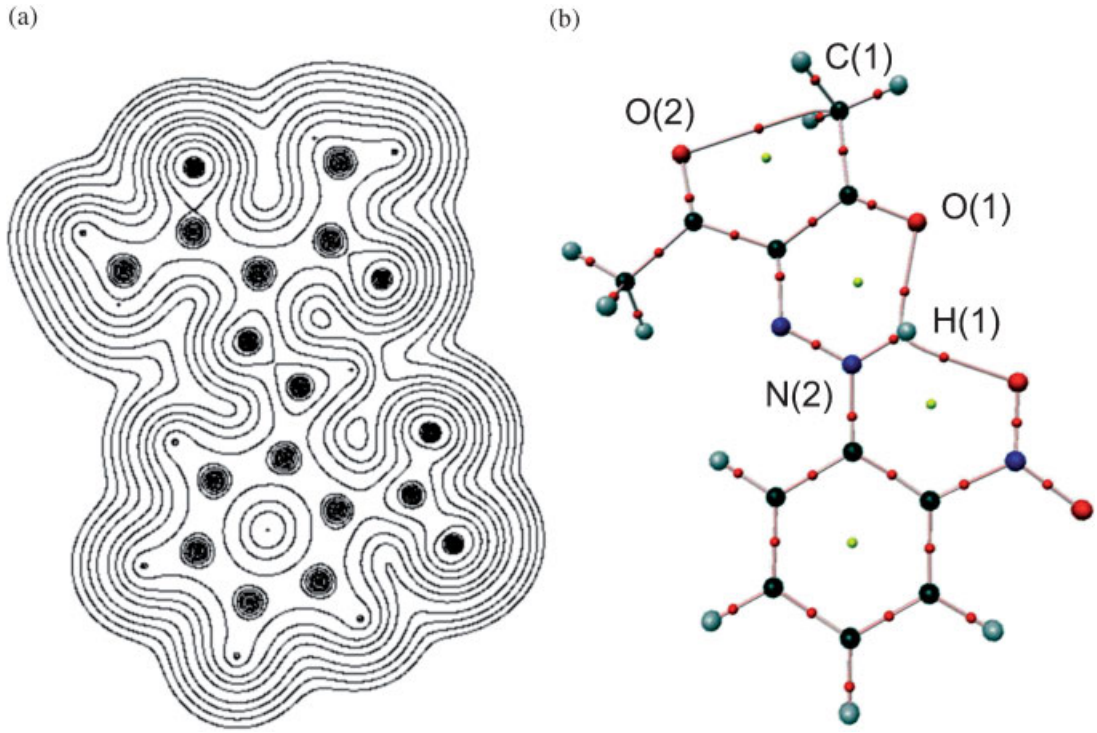

Figure 8. Electron density distribution (a) and representation of bond and ring critical points (b) of **4a**

values of formaldehyde. The low ellipticity of the C═O double bond can be explained with the presence of free electron pairs at the oxygen atom in the plane perpendicular to the π-orbitals of the double bond. The values of the electron density of the C—N-bonds [C(3)—N(1) 0.348 and N(2)—C(6) 0.302 e/Bohr^3] are between the values of methylamine (0.267) and H_2C═NH (0.389), meaning that both bonds of **4a** have partial double bond character; a statement which is supported by the ellipticity. The same is true for the bond N(1)—N(2), when making use of a comparison with the reference molecules hydrazine and HN═NH, that is, a partial double bond character is shown. Three bond critical points between H(2) and its neighboring atoms were found (Table 4). The bond between N(2) and H(2) can be regarded as a typical single covalent bond. There are also bond critical points between H2 and O1 and O3, respectively. The value of electron density at the bond critical point for these interactions is one order of magnitude smaller than for N(2)—H(2). Hence, on the basis of the topological analysis we can assume the presence of hydrogen bonds between these atoms. Similar

Table 4. Electron density and bond ellipticity at selected bond critical points in **4a** and reference molecules

Molecule	Bond critical point	Electron density (e/Bohr^3)	Ellipticity
4a	C(2)–O(1)	0.40	0.074
	C(3)–N(1)	0.348	0.274
	N(2)–C(6)	0.302	0.136
	N(1)–N(2)	0.388	0.105
	N(2)–H(2)	0.322	0.036
	H(2)···O(1)	0.036	0.055
	H(2)···O(3)	0.029	0.071
Ethane	C–C	0.243	0
Ethene	C═C	0.348	0.388
Acetylene	C≡C	0.402	0
Formaldehyde	C═O	0.410	0.072
Methylamine	C–N	0.267	0.041
H_2C═NH	C═N	0.389	0.237
Hydrazine	N–N	0.273	0.037
HN═NH	N═N	0.476	0.17

DOI: 10.1002/poc

values for hydrogen bonds have been found in other molecules.[29,30] A weak interaction is also suggested between O(2) and C(1) based on the presence of a ring critical point (Fig. 8b).

Mixed methyl- and nitro-substituted derivative 6. Two rotamers of **6** are imaginable, depicted as **6a** and **6b** in Fig. 9. The experimentally determined structure in the solid state is similar to the optimized structure **6a**. At the B3LYP/6-311 + G(d,p) level of theory, the optimized geometry **6a** is more stable than **6b**. The energy difference between both rotamers is 4.5 kJ/mol in electronic energy (including zero point correction) and 3.1 kJ/mol in Gibbs free energy. Different effects of steric repulsion are cumulated in this molecule between the substituents in *ortho* position (NO_2 and CH_3) and the hydrazono group. Furthermore, the nitro group is in conjugative interaction with the phenyl ring. The minima at 50 and 130° in the energy profile for the rotation of the nitro group in **6a** (Fig. 10) represent therefore a compromise between minimized steric repulsion and retained conjugative interaction between the nitro group and the phenyl ring. The nitro group and the nitrogen atom N(1) are not able to form any stabilizing orbital interaction. This is shown exemplarily in Fig. 11 with HOMO-2 [free electron pair at N(2)] and HOMO-3 [electron pair at O(3) and O(4) plus phenyl π-orbital].

CONCLUSIONS

As the starting point of this investigation, an *ortho*-mononitro (**4**) and *ortho*-methyl-and nitro-disubstituted arylhydrazone (**6**) were found in unexpectedly different conformations regarding the arylhydrazone bond. Trying to solve this strange behavior, a systematic series of respective *ortho*-mono- and disubstituted arylhydrazones including the unsubstituted parent compound (**1–6**) have been synthesized and studied by X-ray crystal structure analysis, with added quantum chemical calculations.

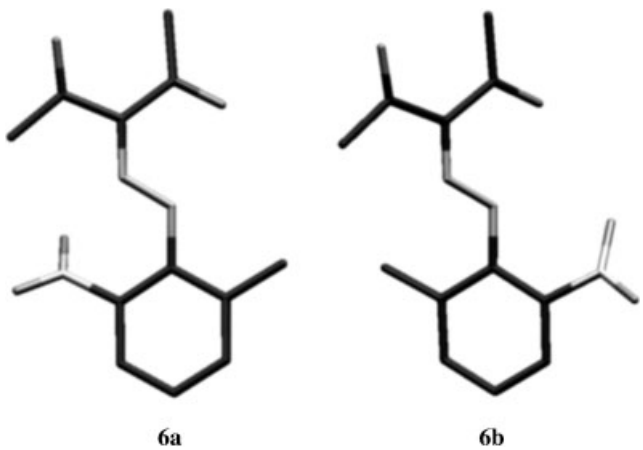

Figure 9. Optimized geometries (B3LYP/6-311 + G(d,p)) of **6a** and **6b**

Due to the good agreement between the optimized geometries based on DFT calculations and the experimental data from crystal structure analysis, relevant rotational barriers could be determined. These give an obvious indication that repulsive forces between an *ortho*-positioned methyl group and the nitrogen-free electron pair are stronger than for a nitro group and the electron pair in this type of molecules, corresponding to the structural findings. Moreover, good correspondence was found between the bond and ring critical points, calculated by the method of 'atoms in molecules' and the experimental data, confirming the conjugate character of the six-membered hydrogen-bonded ring of the hydrazone unit. This is a result not conflicting with the IRAHB model based on π-electron delocalization.[16] Thus, it is shown that DFT calculations carried out on a series of arylhydrazones, formed of pentane-2,4-dione and *ortho*-methyl- and nitro-substituted diazonium salts, are a useful way to make reliable prediction of their molecular conformations. This might be useful in the design of functional materials attributed to smart hydrogen bonding,[11] photo-triggered structural switching,[12] and targeted metal ion complexes.[31]

EXPERIMENTAL

Synthesis

Melting points were determined with a hot-stage microscope (VEB Dresden Analytik) and are uncorrected. Elemental analyses were determined on a Heraeus CHN rapid analyzer. The IR spectra were obtained with a Nicolet 510 FT-IR spectrometer. ^{1}H and ^{13}C-NMR spectra were recorded using a Bruker Avance DPX 400 (400 MHz) instrument. The chemical shifts (δ) are reported as ppm relative to $SiMe_4$. Mass spectra were recorded with a DEI-MS (Finnigan SSQ 710), EI-MS (Bruker Daltonik, ESQUIRE-LC ion trap, solvent: acetonitrile/water/5% formic acid; flow rate 3 µl/min; ion polarity: positive), or GC-MS (Finnigan MAT 8230, source mode: chemical ionization with isobutane, ion polarity: positive).

Compounds 1–6: General procedure

A solution of the diazonium salt was prepared under cooling (0–5 °C) from the respective aniline (20 mmol) in hydrochloric acid (3 N, 40 ml; in the case of compounds **1–4** and **6**) or conc. sulfuric acid (20 ml; for compound **5**) and a conc. aqueous solution of sodium nitrite (1.37 g, 20 mmol) according to the standard procedure.[13] The cold solution of the diazonium salt was added under cooling (0 °C) and stirring to a mixture being composed of

DOI: 10.1002/poc

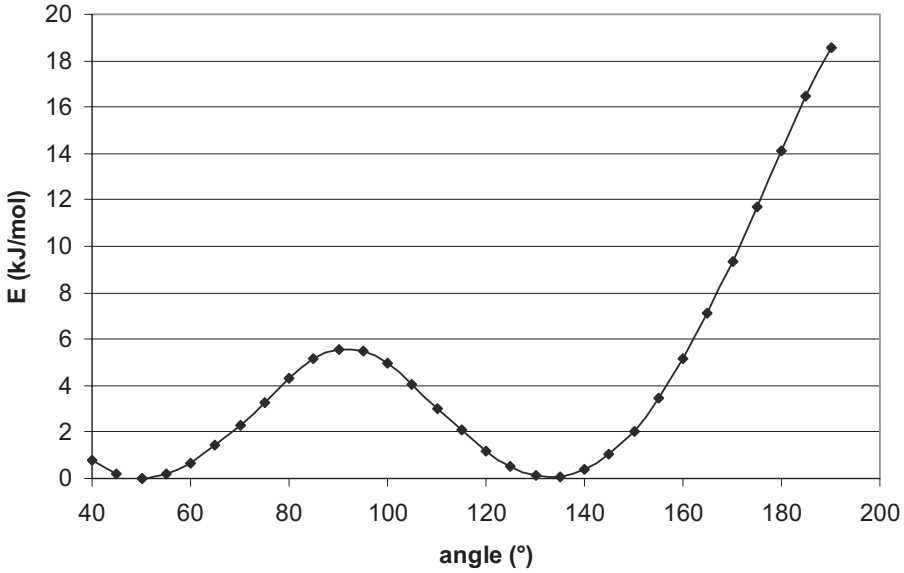

Figure 10. Energy profile for conformational rotation of the nitro group in **6a**

pentane-2,4-dione (2.1 ml, 2.04 g, 20 mmol), NaOH (1.0 g, 25 mmol), sodium acetate (8.2 g, 100 mmol), methanol (160 ml), and water (160 ml). The mixture was allowed to warm to room temperature and stirred for 1 h. The precipitate which had formed was collected, washed with water, and recrystallized from ethanol. Specific details for each compound are given below.

3-(Phenylhydrazono)pentane-2,4-dione (1). Freshly distilled aniline (1.8 ml, 1.86 g, 20 mmol) was used to afford 95% yellow powder; m.p. 85–87 (lit.[32] m.p. 88 °C).

3-(2-Methylphenylhydrazono)pentane-2,4-dione (2). 2-Methylaniline (2.14 g, 20 mmol) was used to afford 96% yellow powder; m.p. 97–99 °C (found, C 65.86, H 6.49, N 12.60; $C_{12}H_{14}N_2O_2$ requires C 66.04, H 6.47, N 12.84%); IR (KBr), $\nu = 3308$ (m, b, N—H), 1669 (s, C═O), 1623 (s, C═O···H), 1584 (s, C═N), 1519 (s, C═C), 1373–1326 (s, CO—CH_3), 760 (s, Ar—H) cm^{-1}; ^{1}H-NMR (400 MHz, $CDCl_3$):$\delta = 2.40$ (s, 3H, CH_3CO), 2.51 (s, 3H, CH_3CO), 2.63 (s, 3H, CH_3), 7.10 (m, $^3J_{H\text{-}H} = 7.6$ Hz, 1H, Ar—H), 7.20 (m, $^3J_{H\text{-}H} = 7.2$ Hz, 1H, Ar—H), 7.28 (m, $^3J_{H\text{-}H} = 7.6$ Hz, 1H, Ar—H), 7.75 (m, $^3J_{H\text{-}H} = 8.0$ Hz, 1H, Ar—H), 14.98 (s, 1H, NH).

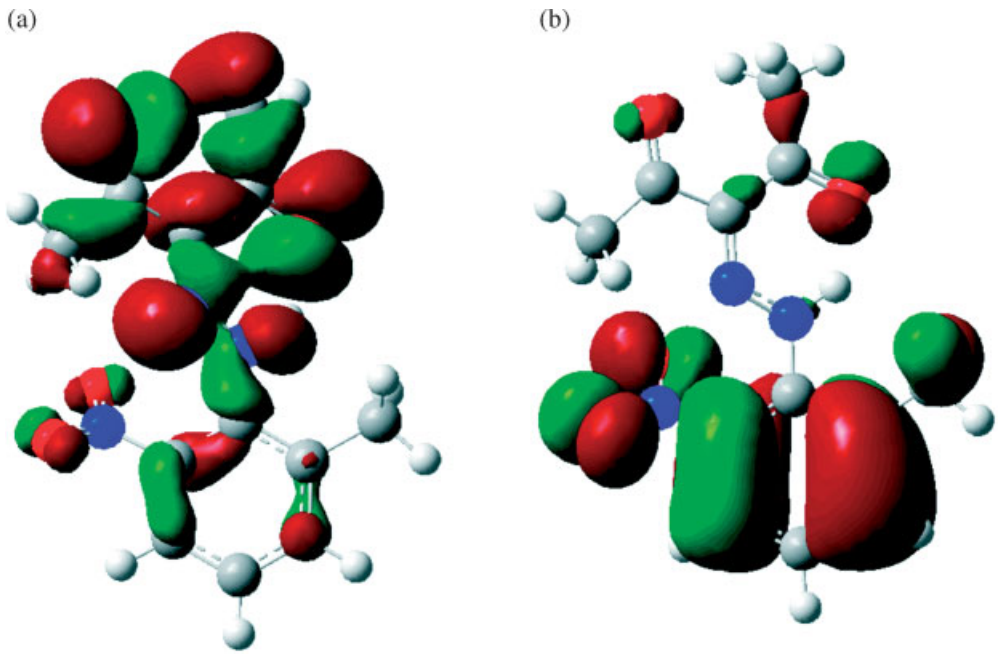

Figure 11. HOMO-2 (a) and HOMO-3 (b) of **6a** (0.02 e/Å^3 isosurface)

DOI: 10.1002/poc

^{13}C-NMR (100.6 MHz, $CDCl_3$):$\delta = 17.00$ (Ar—CH_3), 26.68, 31.56 (CH_3—CO), 115.02 (Ar), 125.68 (C—CH_3), 125.68 (Ar), 127.50 (Ar), 131.09 (Ar), 133.84 (C═N), 139.78 (C—N), 197.19, 197.86 (C═O); MS (GC-MS), $m/z = 218$ $[M + H]^+$ (97%).

3-(2,6-Dimethylphenylhydrazono)pentane-2,4-dione (3). 2,6-Dimethylaniline (2.42 g, 20 mmol) was used to afford 98% yellow powder; m.p. 74–76 °C (found, C 66.96, H 6.94, N 11.89; $C_{13}H_{16}N_2O_2$ requires C 67.22, H 6.94, N 12.06%); IR (KBr), $\nu = 3327$ (m, b, N—H), 1671 (s, C═O), 1616 (s, C═O···H), 1588 (s, C═N), 1522 (s, C═C), 1355–1322 (s, CO—CH_3), 758 (s, Ar—H) cm^{-1}; ^{1}H-NMR (400 MHz, $CDCl_3$): $\delta = 2.40$ (s, 3H, CH_3CO), 2.45 (s, 3H, CH_3CO), 7.07 (m, 2H, Ar—H), 7.12 (m, 1H, Ar—H), 14.97 (s, 1H, NH); ^{13}C-NMR (100.6 MHz, $CDCl_3$): $\delta = 19.38$ (Ar—CH_3), 26.92, 31.54 (CH_3—CO), 126.38 (Ar), 129.66 (Ar), 129.86 (C═N), 133.70 (C—CH_3), 138.07 (C—N), 197.15, 197.65 (C═O); MS (ESI, 150 °C), $m/z = 233$ $[M + H]^+$ (100%).

3-(2-Nitrophenylhydrazono)pentane-2,4-dione (4). 2-Nitroaniline (2.76 g, 20 mmol) was used to afford 99% yellow powder; m.p. 137 °C (found, C 53.05, H 4.64, N 16.86; $C_{11}H_{11}N_3O_4$ requires C 53.01, H 4.45, N 16.50%); IR (KBr), $\nu = 3270$ (m, b, N—H), 1686 (s, C═O), 1643 (s, C═O···H), 1606 (s, C═N), 1494 (s, C═C), 1519 (s, C—NO_2), 1318–1308 (s, CO—CH_3), 790 (s, Ar—H) cm^{-1}; ^{1}H-NMR (400 MHz, $CDCl_3$): $\delta = 2.49$ (s, 3H, CH_3CO), 2.57 (s, 3H, CH_3CO), 7.48 (d, $^3J_{H\text{-}H} = 9.2$ Hz, 2H, Ar—H), 8.29 (d, $^3J_{H\text{-}H} = 9.2$ Hz, 2H, Ar—H), 14.48 (s, 1H, NH). ^{13}C-NMR (100.6 MHz, $CDCl_3$): $\delta = 26.6$, 31.78 (CH_3—CO), 115.80 (Ar), 125.79 (Ar), 15.09 (C═N), 144.61 (C—NO_2), 146.63 (C—N), 196.76, 198.73 (C═O); MS (DEI), $m/z = 249$ $[M + H]^+$ (10%).

3-(2,6-Dinitrophenylhydrazono)pentane-2,4-dione (5). 2,6-Dinitroaniline (3.66 g, 20 mmol) was used to afford 82% yellow powder. In this case we used 20 ml concentrated sulphuric acid instead of the hydrochloric acid; m.p. 153–155 °C (found, C 44.87, H 3.44, N 18.64; $C_{11}H_{10}N_4O_6$ requires C 44.90, H 3.43, N 19.04%); IR (KBr), $\nu = 3266$ (m, b, N—H), 1675 (s, C═O), 1617 (s, C═O···H), 1538 (s, C═C), 1504 (s, C—NO_2), 1360–1320 (s, CO—CH_3), 740 (s, Ar—H) cm^{-1}; ^{1}H-NMR (400 MHz, $CDCl_3$): $\delta = 2.39$ (s, 3H, CH_3CO), 2.63 (s, 3H, CH_3CO), 8,18 (m, $^3J_{H\text{-}H} = 8.0$ Hz, 2H, Ar—H), 8.36 (m, $^3J_{H\text{-}H} = 8.4$ Hz, 1H, Ar—H), 15.17 (s, 1H, NH); ^{13}C-NMR (100.6 MHz, $CDCl_3$): $\delta = 26.36$, 31.77 (CH_3—CO), 120.36 (Ar), 130.25 (Ar), 132.82 (C—NO_2), 137.64 (C═N), 142.27 (C—N), 197.01, 198.04 (C═O); MS (GC-MS), $m/z = 294$ $[M + H]^+$ (100%).

3-(2-Methyl-6-nitrophenylhydrazono)pentane-2,4-dione (6). 2-Methyl-6-nitroaniline (3.04 g, 20 mmol) was used to afford 98% yellow powder; m.p. 99 °C (found, C 55.05, H 5.02, N 15.88; $C_{12}H_{13}N_3O_4$ requires C 54.75, H 4.98, N 15.96%); IR (KBr), $\nu = 3330$ (m, b, N—H), 1675 (s, C═O), 1635 (s, C═O···H), 1606 (s, C═N), 1535 (s, C═C), 1359–1308 (s, CO—CH_3), 791 (s, Ar—H) cm^{-1}; ^{1}H-NMR (400 MHz, $CDCl_3$): $\delta = 2.33$ (s, 3H, CH_3CO), 2.49 (s, 3H, CH_3CO), 2.63 (m, 3H, C—CH_3), 7.31 (m, 1H, Ar), 7.63 (d, $^3J_{H\text{-}H} = 7.6$ Hz, 1H, Ar—H), 7.8 (d, $^3J_{H\text{-}H} = 8.4$ Hz, 1H, Ar—H), 14.26 (s, 1H, NH); ^{13}C-NMR (100.6 MHz, $CDCl_3$): $\delta = 19.00$ (CH_3), 26.49, 31.70 (CH_3—CO), 123.51 (Ar), 125.14 (Ar), 133.43 (C—CH_3), 135.30 (C—NO_2), 135.31 (C═N), 135.44 (Ar), 141.64 (C—N), 197.11, 197.33 (C═O); MS (ESI, 150 °C), $m/z = 264$ $[M + H]^+$ 40%).

X-ray crystallography

The X-ray diffraction data of **3** and **6** were collected on a CAD-4 diffractometer in the ω–2θ scan mode ($\lambda_{CuK\alpha} = 1.5418$ Å, graphite monochromator). X-ray diffraction studies of **1**, **2**, **4**, and **5** were carried out on a Bruker-AXS APEX II diffractometer with a CCD area detector ($\lambda_{MoK\alpha} = 0.71073$ graphite monochromator): Frames were collected with ω and ϕ rotation at 10 s per frame. The net intensities were corrected for Lorentz and polarization effects. Absorption correction was carried out with SADABS (SAINT-NT).[33] Preliminary structure models were derived by application of direct methods [34] and were refined by full-matrix least-squares calculation based on F^2 values for all unique reflections. The non-hydrogen atom positions were refined anisotropically. The nitrogen-bonded hydrogen atom H(2) in **3** and **6** was included in the models in calculated positions, whereas this hydrogen in structures **1**, **2**, **4**, and **5** was extracted from difference electron density maps and was hold riding on its parent nitrogen atom during subsequent calculations.

Supplementary material

Crystallographic data for the structures in this paper have been deposited with the Cambridge Crystallographic Data Centre as supplementary publication numbers CCDC-633705 (**1**), CCDC-633706 (**2**), CCDC-633707 (**3**), CCDC-633708 (**4**) CCDC-633709 (**5**), and CCDC-255318 (**6**). Copies of the data can be obtained, free of charge, on application to CCDC, 12 Union Road, Cambridge CB2 1EZ, UK (fax: +44-1223-336033, e-mail: deposit@ccdc.cam.ac.uk).

Quantum chemical calculations

The Quantum chemical calculations were carried out using the GAUSSIAN 03 series of programs.[35] Geometries were fully optimized at the density functional theory

DOI: 10.1002/poc

level (DFT), using Becke's three-parameter hybrid exchange functional and the correlation functional of Lee, Yang, and Parr (B3LYP).[36,37] Geometry optimizations and harmonic frequencies were calculated for all elements with the polarized 6-31G(d,p) basis set for **2a–5a** and with the 6-311 + G(d,p) basis set for **6a** and **6b**.[19,38,39] The stationary points were characterized by zero imaginary frequencies.

Relaxed PES scans have been performed with the Opt = ModRedundant utility in Gaussian 03 with B3LYP/6-311 + G(d,p). This option includes the specification of redundant internal coordinates. In these cases, a specific torsion angle has been changed in five degree steps. On every step, the geometry of the molecule was completely optimized, restricting only the torsion angle to the specified value. This method allows access to a defined section of the PES. Rotational barriers which include the breaking and formation of hydrogen bonds strongly depend from the basis set. Therefore, different basis sets in combination with the B3LYP functional have been tested for that purpose: 6-31G(d,p); 6-31 + G(d,p); 6-311 + G(d,p). The lowest and probably most realistic barrier was obtained with B3LYP/6-311 + G(d,p). The calculation of the PES scans included up to 36 optimization steps. Therefore, the use of computational expensive electron correlation methods like CCSD or MP2 is impractical. The same holds for more extensive basis sets. DFT methods fail to describe any stabilization originated from the dispersion energy.[40] Therefore, one should keep in mind that the presented PES profiles represent estimations of the rotational barriers.

Three-dimensional MO plots were generated with GaussView [41] with a contour value of 0.02 e/Å^3. The AIM analyses[22] of **4a** and the reference molecules have been performed at the B3LYP/6-311 + G(2d,p) level with the previously optimized geometries and could be denoted as: B3LYP/6-311 + G(2d,p)//(B3YLP/6-31G(d,p). The wavefunction files for the AIM analysis were generated in Cartesian coordinates with a basis set containing 6d functions. The option SCF = Tight was used to prevent 'charge leakage' as described by Popelier.[42] The electron density topology was analyzed using the AIMPAC programs which can be obtained from the official Atoms in Molecules Download Site at http://www.chemistry.mcmaster.ca/aimpac/ and AIM2000 by F. Biegler-König and J. Schönbohm.

Acknowledgements

We gratefully acknowledge financial support by the German Ministry of Science and Technology (BMBF-Project 'BioMon' 02110120).

REFERENCES

1. Phillips RR. *Org. React.* 1959; **10**: 143–178.
2. Bertolasi V, Ferretti V, Gilli P, Gilli G, Issa YM, Sherif OM. *J. Chem. Soc., Perkin Trans. 2* 1993; 2223–2228.
3. Marten J, Seichter W, Weber E. *Z. Anorg. Allg. Chem.* 2005; **631**: 869–877.
4. Albert J, Gonzales A, Granell J, Moragas R, Puerta C, Valerla P. *Organometallics* 1997; **16**: 3775–3778.
5. Mishra L, Yadaw AK, Srivastava S. *New J. Chem.* 2000; **24**: 505–510.
6. Kuzmina NP, Eliseeva SV, Balashov AM, Trojanov SI. *Z. Neorg. Chim. Moscow* 2002; **47**: 1300–1304.
7. Sharma G. *J. Med. Chem.* 1969; **12**: 1122–1124.
8. Bertolasi V, Nanni L, Gilli P, Ferretti V, Gilli G. *New. J. Chem.* 1994; **18**: 251–261.
9. Yao HC. *J. Chem. Soc.* 1964; 2959–2963.
10. Rappoport H. *The Chemistry of Enols*. Wiley: New York, 1990.
11. Gilli P, Bertolasi V, Pretto L, Lyčka A, Gilli G. *J. Am. Chem. Soc.* 2002; **124**: 13554–13567.
12. McVie J, Alastair D, Sinclair RS, Truscott TG. *J. Chem. Soc. Perkin Trans.* 1980; **2**: 286–290.
13. Püttner R. In *Methoden der Organischen Chemie. (Houben-Weyl)*, vol. **10/3**: 1965; p. 1.
14. Gilli G, Belucci F, Ferretti V, Bertolasi V. *J. Am. Chem. Soc.* 1989; **111**: 1023–1028.
15. Elguero J, Mo O, Yanez M, del Bene JE. *Mol. Phys.* 2004; **102**: 2563–2571.
16. Grabowski SJ. *J. Phys. Org. Chem.* 2003; **16**: 797–802.
17. Sanchez AG, de Gracia M, Garcia M, Borrachero P, Bellanato J. *J. Chem. Soc., Perkin Trans. 2* 1987; 301–306.
18. Gawinecki R, Kolehmainen E, Janota H, Kauppinen R, Nissinen M, Osmialowski B. *J. Phys. Org. Chem.* 2001; **14**: 797–803.
19. Hehre WJ, Radom L, Schleyer PR, Pople JA. *Ab Initio Molecular Orbital Theory.* J. Wiley & Sons: Chichester, 1986.
20. The rotational barriers in nitrobenzol and other aromatic nitro compounds have been investigated before; for further details see: Chen PC, Chen SC, *Int. J. Quantum Chem.* 2001; **83**: 332–337.
21. Gilli P, Bertolasi V, Ferretti V, Gilli G. *J. Am. Chem. Soc* 2000; **122**: 10405–10417.
22. Bader RFW. *Atoms in Molecules*. Clarendon Press: Oxford, 1994.
23. Gillespie RJ. *J. Chem. Educ.* 2001; **78**: 1688–1690.
24. Explanation taken from: Gillespie RA, Popelier PLA, *Chemical Bonding and Molecular Geometry*. Oxford University Press: New York, 2001.
25. Matta CF, Hernández-Trujillo J, Tang TH, Bader RFW. *Chem. Eur. J.* 2003; **9**: 1940–1951.
26. Poater J, Solà M, Bickelhaupt FM. *Chem. Eur. J.* 2006; **12**: 2889–2895.
27. Bader RFW. *Chem. Eur. J.* 2006; **12**: 2896–2901.
28. Poater J, Solà M, Bickelhaupt FM. *Chem. Eur. J.* 2006; **12**: 2902–2905.
29. Espinosa E, Souhassou M, Lachekar H, Lecomte C. *Acta Cryst.* 1999; **B55**: 563–572.
30. Aydeniz Y, Oguz F, Yaman A, Konuklar AS, Dogan I, Aviyente V, Klein RA. *Org. Biomol. Chem.* 2004; **2**: 2426–2436.
31. McCleverty JA, Meyer TJ, Fujita M, Powell A, Creutz CA. *Comprehensive Coordination Chemistry.* Elsevier: Oxford, 2004.
32. Ho YW, Wang IJ. *Dyes Pigments* 1995; **29**: 295–304.
33. Bruker Analytical X-ray, Systems. *SAINT-NT* (Version 6.0), 2003.
34. Sheldrick GM. *SHELX-97, Program for Crystal Structure Solution and Refinement*. University of Göttingen: Germany, 1997.
35. Gaussian 03, Revision C.02, Frisch MJ, Trucks GW, Schlegel HB, Scuseria GE, Robb MA, Cheeseman JR, Montgomery JA, Vreven T, Kudin KN, Burant JC, Millam JM, Iyengar SS, Tomasi J, Barone V, Mennucci B, Cossi M, Scalmani G, Rega N, Petersson GA, Nakatsuji H, Hada M, Ehara M, Toyota K, Fukuda R, Hasegawa J, Ishida M, Nakajima T, Honda Y, Kitao O, Nakai H, Klene M, Li X, Knox JE, Hratchian HP, Cross JB, Adamo C, Jaramillo J, Gomperts R, Stratmann RE, Yazyev O, Austin AJ, Cammi R, Pomelli C, Ochterski JW, Ayala PY, Morokuma K, Voth GA, Salvador P, Dannenberg JJ, Zakrzewski VG, Dapprich S, Daniels AD, Strain MC, Farkas O, Malick DK, Rabuck AD, Raghavachari K, Foresman JB, Ortiz JV, Cui Q, Baboul AG, Clifford S, Cioslowski J, Stefanov BB, Liu G, Liashenko A, Piskorz P, Komaromi I, Martin RL, Fox DJ, Keith T, Al-Laham MA, Peng CY, Nanayakkara A, Challacombe M, Gill PMW, Johnson B, Chen W, Wong MW, Gonzalez C, Pople JA. Gaussian, Inc.: Wallingford CT, 2004.

DOI: 10.1002/poc

36. Becke AD. *J. Chem. Phys.* 1993; **98**: 5648–5652.
37. Stephens PJ, Devlin FJ, Chabalowski CF, Frisch MJ. *J. Phys. Chem.* 1994; **98**: 11623–11627.
38. Hariharan PC, Pople JA. *Theoret. Chimica Acta.* 1973; **28**: 213–222.
39. Francl MM, Pietro WJ, Hehre WJ, Binkley JS, Gordon MS, DeFrees DJ, Pople JA. *J. Chem. Phys.* 1982; **77**: 3654–3665.
40. Hobza P. *Annu. Rep. Prog. Chem., Sect. C* 2004; **100**: 3–27.
41. GaussView 3.0, Gaussian Inc., Pittsburgh 2004.
42. Popelier LA. *Comput. Phys. Commun.* 1998; **108**: 180–190.

DOI: 10.1002/poc